Coupled-mode equations for quadratically nonlinear deep gratings

Awdah Arraf* and C. Martijn de Sterke
School of Physics, University of Sydney, Sydney, New South Wales 2006, Australia
and Australian Photonics Cooperative Research Centre, 101 National Innovation Centre, Australian Technology Park, Eveleigh, New South Wales 1430, Australia
(Received 24 March 1998)

Using the method of multiple scales, we present a systematic derivation of the coupled-mode equations for the propagation of light in quadratically nonlinear deep gratings. We show that the resulting coupled-mode equations for deep gratings differ from those for shallow gratings in that the coefficients have different values, and that additional nonlinear terms appear. Our equations reduce to well known results, in the appropriate shallow grating limit. [S1063-651X(98)07512-6]

PACS number(s): 42.65.Ky

I. INTRODUCTION

A particularly interesting feature of the properties of periodic Kerr media is the possibility of observing soliton propagation. Optical grating solitons are high-intensity nonlinear pulses which can maintain their shape upon propagation in a grating [1]. The field structure in such pulses maintains its stability through a counterbalancing of the effect of the Kerr nonlinearity, which concentrates the pulse energy, and the effect of group velocity dispersion, which disperses it, induced by the periodic structure [1]. Such optical pulses occur at frequencies around the photonic band gap which is centered at the Bragg frequency associated with the periodicity of the structure [1]. Optical grating solitons have been studied theoretically for many years; however, it was not until a few years ago that they were observed experimentally in an optical fiber Bragg grating of a few centimeters in length [2]. This length should be contrasted with temporal solitons in uniform fibers, which typically require lengths of 100's of meters [3,4]. The difference in the length scales arises from the grating dispersion, which is several orders of magnitude larger than that of a uniform fiber.

In second harmonic generation (SHG), the cascaded up and down conversion, in the limit of a large wave vector mismatch between the fundamental frequency (FF) and the second harmonic frequency (SHF), can lead to similar nonlinear phase shifts as those obtained in Kerr nonlinear materials [5]. Soliton propagation in quadratically nonlinear media has been of particular interest in recent years leading to many theoretical results on a variety of parametric solitons [6–11]. In addition to the theoretical work, evidence of the propagation of spatial and temporal solitons in quadratically nonlinear media has also been confirmed experimentally [12–16]. The spatial solitons reported in Ref. [12] were demonstrated through type II SHG (where the two FF beams are orthogonally polarized) in a 1-cm-long potassium titanyl phosphate (KTP) crystal. Temporal solitons were observed in a 7-mm-long β-barium borate crystal in which the tilt of the pulse's amplitude front with respect to its phase front compensates for the group velocity mismatch, and introduces strong anomalous dispersion [16].

As mentioned, Bragg gratings can also provide the strong dispersion required for the propagation of temporal solitons [2]. Gratings also offer considerable flexibility in design; by choosing the appropriate grating period one can, in principle, shift the grating dispersion to any spectral region of interest. The promise of the availability of quadratically nonlinear gratings has motivated a number of theoretical publications on the propagation of temporal solitons in quadratically nonlinear media in the presence of shallow gratings [9–11]. In addition to these geometries, Conti, Trillo, and Assanto [17] analytically considered nonlinear propagation in the presence of quadratically nonlinear deep gratings. In their work they used a Bloch function approach to derive two Schrödinger equations which are known to possess solitary wave solutions. Also, more recently, Scalora *et al.* [18] considered pulsed SHG in nonlinear, one-dimensional, deep, periodic structures. However, to our knowledge, there has been no analytical derivation of general coupled-mode equations for the propagation of electromagnetic waves in quadratically nonlinear deep gratings. Here we consider such structures, and rigorously derive the evolution equations for the fields in such geometries. This leads to a generalization of the result for shallow gratings in Refs. [9–11].

Although our treatment, strictly speaking, applies only to periodic thin-film stacks, in guided-wave structures it is almost always possible to avoid the explicit dependence of the fields on the transverse coordinates. In making such an approximation one assumes that the modal profiles in the transverse direction are not affected by the periodicity of the refractive index or the nonlinearity; under these assumptions the problem becomes one dimensional, and it can then be treated using the method developed here [4,19]. One-dimensional problems can also be solved exactly by integrating the Maxwell equations [20]. However, one can gain more physical insight into the problem by using a coupled-mode theory formalism. When this method is applied to periodic structures, the relevant modes are often taken to be the forward and backward propagating modes of the associated linear, uniform medium (or, in other words, the eigenmodes), while the grating and the nonlinearity act as a perturbation coupling these two modes. However, since the grating acts as

*Fax: 61 2 9351 7726. Electronic address: a.arraf@physics.usyd.edu.au

a perturbation, this method can only be used for shallow gratings. When the grating is deep, the relevant modes cannot simply be taken to be the forward and backward propagating modes, but must be the Bloch functions of the periodic structure. An extension of standard coupled-mode theory, in which the fields are expanded into Bloch functions, has recently been developed for deep gratings with a cubic nonlinearity [21]. This treatment involves deriving a set of coupled-mode equations which are similar, in the appropriate limit, to those that follow from conventional coupled-mode theory. The approach used in Ref. [21] relies on expanding the field envelopes in the Bloch functions of the corresponding linear structure. Here we adapt this approach so that it can be applied to treat quadratically nonlinear deep gratings. Since we have two frequencies and two propagation directions, this leads to a set of four coupled equations [9–11]. In contrast, a deep grating with a cubic nonlinearity leads to two coupled-mode equations [21].

The content of the paper is as follows. In Sec. II we derive the coupled envelope function equations for quadratically nonlinear deep gratings which, using the transformation given in Sec. III, can be written in a standard form. Then, in Sec. IV, we discuss some relevant properties of Bloch functions. In Sec. V we consider the shallow grating limit of our results, and show that the resulting equations are consistent with those derived in the literature. The nonlinear coefficients for quadratically nonlinear deep gratings are evaluated and discussed in Sec. VI. Finally, conclusions are drawn in Sec. VII.

II. NONLINEAR COUPLED ENVELOPE FUNCTION EQUATIONS

In this section we present a derivation of the coupled envelope function equations at the FF and SHF for light propagating in a quadratically nonlinear deep grating. The details of the procedure we use were described in Secs. VI A and VI B of Ref. [21], and thus are not repeated here.

Following earlier work [9–11], we consider scalar type I SHG where a single FF beam is launched onto a quadratically nonlinear medium, but now in the presence of a deep grating rather than a shallow one. The FF field is taken to be tuned to a frequency close to the center ω_{10} of the first grating-induced band gap. This leads to a SHF which lies in the vicinity of the center ω_{20} of the second grating-induced band gap. Note that because of the material's dispersion, $\omega_{20} \neq 2\omega_{10}$. To expand the field envelopes into the Bloch functions of the linear structure, we must consider the positions of the band gaps in the Brillouin zone (BZ). Figure 1 shows a typical photonic band structure in the first BZ.

In Fig. 1 the semicircle (on the right hand side) and the circle (in the center) indicate the FF and SHF band gaps, respectively; these are also labeled with 1 and 2. Clearly, the first and the second grating-induced band gaps occur at the edge and center of the first BZ. Also shown in Fig. 1 is a typical range of frequencies for the FF and SHF fields. For the FF field, this range is the shaded region just below ω_{10}. This leads to a SHF field with a range of frequencies which is twice as broad, and is indicated by the shaded region just below ω_{20}.

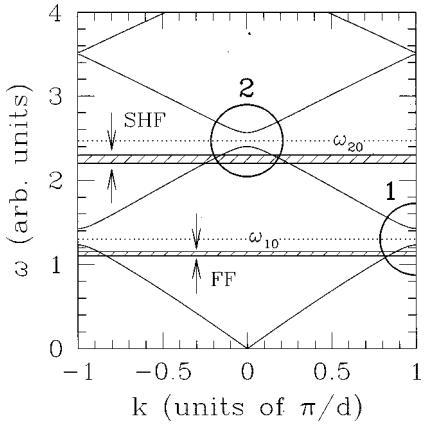

FIG. 1. Schematic of a photonic band structure of a deep grating, showing the angular frequency ω as a function of the reduced wave number k in the first BZ ($-\pi/d < k \leq \pi/d$). The shaded regions are typical ranges of frequencies for the FF and the SHF fields. The circle and semicircle indicate the SHF and FF band gaps, respectively.

An enlarged schematic of the two relevant band gaps is shown in Fig. 2. The band gaps are bounded by $\omega_{ml,u}$. Here, and throughout this paper, the subscript $m=1$ and 2, where 1 and 2 refer to the FF and SHF or the first and the second grating-induced band gaps, respectively. The subscripts l and u refer to the lower and upper band edges of each band gap, respectively. Since ω_{m0} is at the center of each of these band gaps we must have

$$\omega_{m0} = \tfrac{1}{2}(\omega_{ml} + \omega_{mu}). \tag{1}$$

We consider an electric field as in Fig. 1 (dashed regions), in which the FF and the SHF spectral components are well separated. We designate these electric field components as E_1 and E_2, respectively, and similarly for the magnetic field H. Rather than working with these actual fields it is more convenient to introduce the local mode amplitudes. Recall that, in a uniform medium, two waves, at the FF and its SHF, traveling toward $z=+\infty$ would have magnetic and electric fields related by $H_m = n_m E_m / \mathcal{Z}_0$, where $\mathcal{Z}_0$ is the vacuum

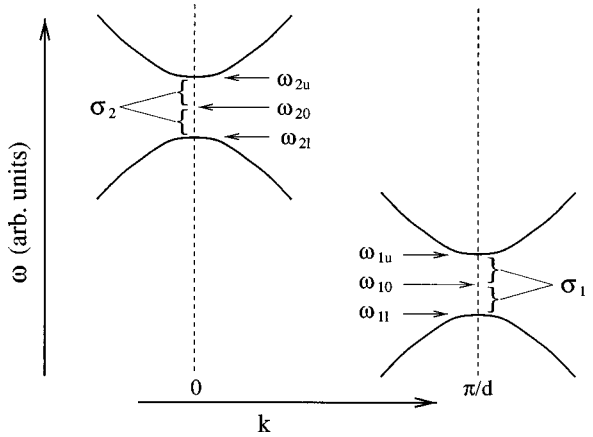

FIG. 2. Schematic showing the FF and the SHF band gaps, at $k=\pi/d$ and $k=0$ in the first BZ. The center frequencies ω_{10} and ω_{20} are halfway between the band gap edges at ω_{ml} and ω_{mu}.

impedance, while those traveling toward $z=-\infty$ would have $H_m=-n_mE_m/\mathcal{Z}_0$. Thus, we can introduce [21,22]

$$A_{m\pm}=\frac{1}{2}\left[\frac{n_m(z)}{n_0}\right]^{1/2}\left[E_m(z,t)\pm\mathcal{Z}_0\frac{H_m(z,t)}{n_m(z)}\right], \tag{2}$$

where $A_{m+}(z)$ is related to the component of the field propagating in the forward direction, and $A_{m-}(z)$ to that propagating in the backward direction. The factor $[n_m(z)/n_0]^{1/2}$, where n_0 is a reference refractive index and where $n_m(z)$ is the spatially dependent refractive index at the relevant frequency, is introduced because the flux carried by plane waves in a uniform medium is proportional to $n_m|E_m|^2=|\sqrt{n_m}E_m|^2$. With the definitions in Eqs. (2) we thus expect the flux toward $z=+\infty$ to be described by $\Sigma(|A_{m+}(z)|^2)$, and that toward $z=-\infty$ to be described by $\Sigma(|A_{m-}(z)|^2)$. As an aside, we note that for a structure with transverse dependence, the refractive indices are understood to be effective indices, corresponding to a suitably weighted transverse average, determined by the modal profile.

We write $\mathbf{A}_m=[A_{m+},A_{m-}]$ as combinations of two eigenvectors and two slowly varying envelopes [21],

$$\mathbf{A}_m=[f_{ml}\boldsymbol{\Psi}_{ml}+f_{mu}\boldsymbol{\Psi}_{mu}]e^{-i\omega_{m0}t}+\text{c.c.}, \tag{3}$$

where $f_{ml,u}$ are the slowly varying envelopes, and the eigenvectors $\boldsymbol{\Psi}_{ml,u}=[\psi^{+}_{ml,u},\psi^{-}_{ml,u}]$ are [21]

$$\psi^{\pm}_{ml,u}(z)=\frac{1}{2}\left[\sqrt{n_m(z)}\,\phi_{ml,u}(z)\mp\frac{ic}{\omega_{ml,u}}\frac{1}{\sqrt{n_m(z)}}\frac{\partial\phi_{ml,u}(z)}{\partial z}\right], \tag{4}$$

where $\phi_{ml,u}$ are the Bloch functions at the relevant band gap edge, and c is the speed of light in vacuum.

Substituting Eqs. (2) into the Maxwell equations, we can derive the equations which are satisfied by the $A_{m\pm}$,

$$i\mathbf{n}_m\cdot\frac{\partial\mathbf{A}_m}{\partial t}=\mathbf{M}_m\cdot\mathbf{A}_m+\mathbf{B}_m, \tag{5}$$

where the refractive index $\mathbf{n}_m$ is given by

$$\mathbf{n}_m=\begin{bmatrix} n_m(z) & 0\\ 0 & n_m(z)\end{bmatrix}, \tag{6}$$

and the matrix differential operator $\mathbf{M}_m$ has the form

$$\mathbf{M}_m=\begin{bmatrix} -ic\dfrac{\partial}{\partial z} & \dfrac{1}{2}ic\dfrac{\partial[\ln n_m(z)]}{\partial z}\\ -\dfrac{1}{2}ic\dfrac{\partial[\ln n_m(z)]}{\partial z} & ic\dfrac{\partial}{\partial z}\end{bmatrix}. \tag{7}$$

Finally, in Eq. (5), $\mathbf{B}_m$ results from the nonlinear polarization, and is defined below.

Starting from Eqs. (5), we use the method of multiple scales established in Ref. [21] to derive the coupled-mode equations. In this formalism, one defines a set of multiple scales for the problem, which can then be used to keep track of the variations in each of the amplitudes, the nonlinearity, and the Bloch functions of the structure considered. By substituting Eqs. (3) into Eqs. (5), and collecting all the terms that vary on the same scales, it can be shown that the field envelopes satisfy the coupled equations

$$\begin{aligned} i\frac{\partial f_{mu}}{\partial t}&=+\sigma_m f_{mu}-iv_{mul}\frac{\partial f_{ml}}{\partial z}+\frac{1}{N}(\boldsymbol{\Psi}^{\dagger}_{mu}\cdot\mathbf{B}_m)e^{i\omega_{m0}t},\\ i\frac{\partial f_{ml}}{\partial t}&=-\sigma_m f_{ml}-iv_{mlu}\frac{\partial f_{mu}}{\partial z}+\frac{1}{N}(\boldsymbol{\Psi}^{\dagger}_{ml}\cdot\mathbf{B}_m)e^{i\omega_{m0}t},\end{aligned} \tag{8}$$

where $N=L/d$ is a normalization constant. Here d is the period of the grating and L is the length over which the Bloch functions are normalized. We note that the final results, presented in Sec. III, do not depend on L, as required. Further, σ_m, as indicated in Fig. 2, is the detuning of the frequencies at the band edges from the center of the band gaps, and is given by

$$\sigma_m=\omega_{mu}-\omega_{m0}=\omega_{m0}-\omega_{ml}, \tag{9}$$

where the last equality follows from Eq. (1). The velocity matrix element $v_{mlu}=-v_{mul}$ is given by [21]

$$\frac{v_{mlu}}{c}=\frac{-ic}{2N}\left(\frac{1}{\omega_{mu}}+\frac{1}{\omega_{ml}}\right)\int_0^L\phi^{*}_{ml}(z)\frac{\partial\phi_{mu}(z)}{\partial z}dz. \tag{10}$$

In Eqs. (8), $\mathbf{B}_m$, which was introduced in Eq. (5), has two identical components given by [21]

$$B_{m\pm}(z,t)=-\frac{i}{2\epsilon_0\sqrt{n_0n_m(z)}}\frac{\partial P_{mNL}}{\partial t}. \tag{11}$$

In the last terms in Eqs. (8), we only include the terms which vary on the same scale as the rest of the terms in Eqs. (8). For type I SHG, where the FF field is linearly polarized, these terms are [23–25]

$$\begin{aligned} P_{1NL}(z,t)&=2\epsilon_0\chi^{(2)}_{\text{eff}}(z)E^{*}_1(z,t)E_2(z,t),\\ P_{2NL}(z,t)&=\epsilon_0\chi^{(2)}_{\text{eff}}(z)E^{2}_1(z,t),\end{aligned} \tag{12}$$

where $\chi^{(2)}_{\text{eff}}$ represents the effective second-order nonlinear susceptibility [23,24], which is a suitably weighted average over the elements of the $\chi^{(2)}$ tensor, and which is determined by the polarization directions of the fields, and the point group of the material. Though phase matching is not required here, it determines the magnitude of $\chi^{(2)}_{\text{eff}}$. Further, $\chi^{(2)}_{\text{eff}}$ can be uniform or vary with the same period as $n_m(z)$. Expressing $E(z,t)$ in terms of $A_{m\pm}(z,t)$ from Eqs. (2), we find

$$E_m=\left[\frac{n_0}{n_m(z)}\right]^{1/2}[A_{m+}(z,t)+A_{m-}(z,t)]. \tag{13}$$

With this expression for $E_m(z,t)$, Eqs. (11) become

$$\begin{aligned} B_{1\pm}&=-i\frac{\chi^{(2)}_{\text{eff}}n_0^{1/2}}{n_1(z)\sqrt{n_2(z)}}\frac{\partial}{\partial t}\{[A^{*}_{1+}(z,t)+A^{*}_{1-}(z,t)]\\ &\quad\times[A_{2+}(z,t)+A_{2-}(z,t)]\},\\ B_{2\pm}&=-i\frac{\chi^{(2)}_{\text{eff}}n_0^{1/2}}{2n_1(z)\sqrt{n_2(z)}}\frac{\partial}{\partial t}\{[A_{1+}(z,t)+A_{1-}(z,t)]^2\}.\end{aligned} \tag{14}$$

Further, using Eqs. (2) in Eqs. (13), $E_m(z,t)$ can be expressed directly in terms of the slowly varying amplitudes f_{mu} and f_{ml}, and the Bloch functions ϕ_{ml} and ϕ_{ul} as

$$E_m = n_0^{1/2}(f_{ml}\phi_{ml} + f_{mu}\phi_{mu})e^{-i\omega_{m0}t} + \text{c.c.} \tag{15}$$

Substituting Eqs. (15) into Eqs. (14) leads to the complete expression of the nonlinearity which is given by

$$\begin{aligned} B_{1\pm} = & \frac{-n_0{}^{1/2}(\omega_{20}-\omega_{10})\chi^{(2)}_{\text{eff}}(z)}{\sqrt{n_1(z)}} \\ & \times (f^*_{1u}f_{2u}\phi^*_{1u}\phi_{2u} + f^*_{1u}f_{2l}\phi^*_{1u}\phi_{2l} \\ & + f^*_{1l}f_{2u}\phi^*_{1l}\phi_{2u} + f^*_{1l}f_{2l}\phi^*_{1l}\phi_{2l})e^{-i(\omega_{20}-\omega_{10})t}, \\ B_{2\pm} = & \frac{-n_0{}^{1/2}\omega_{10}\chi^{(2)}_{\text{eff}}(z)}{\sqrt{n_2(z)}} \\ & \times (f^2_{1u}\phi^2_{1u} + f^2_{1l}\phi^2_{1l} + f_{1u}f_{1l}\phi_{1u}\phi_{1l})e^{-2i\omega_{10}t}. \end{aligned} \tag{16}$$

With Eqs. (16) in Eqs. (8) we find

$$\begin{aligned} i\frac{\partial f_{1u}}{\partial t} = & +v_{1g}\frac{\partial f_{1l}}{\partial z} + \sigma_1 f_{1u} - (\alpha^*_{1u1u2u}f^*_{1u}f_{2u} + \alpha^*_{1u1u2l}f^*_{1u}f_{2l} \\ & + \alpha^*_{1u1l2u}f^*_{1l}f_{2u} + \alpha^*_{1u1l2l}f^*_{1l}f_{2l})e^{-i\delta t}, \\ i\frac{\partial f_{1l}}{\partial t} = & -v_{1g}\frac{\partial f_{1u}}{\partial z} - \sigma_1 f_{1l} - (\alpha^*_{1l1u2u}f^*_{1u}f_{2u} + \alpha^*_{1l1u2l}f^*_{1u}f_{2l} \\ & + \alpha^*_{1l1l2u}f^*_{1l}f_{2u} + \alpha^*_{1l1l2l}f^*_{1l}f_{2l})e^{-i\delta t}, \\ i\frac{\partial f_{2u}}{\partial t} = & +v_{2g}\frac{\partial f_{2l}}{\partial z} + \sigma_2 f_{2u} - (\alpha_{1u1u2u}f^2_{1u} + \alpha_{1l1l2u}f^2_{1l} \\ & + 2\alpha_{1u1l2u}f_{1u}f_{1l})e^{+i\delta t}, \\ i\frac{\partial f_{2l}}{\partial t} = & -v_{2g}\frac{\partial f_{2u}}{\partial z} - \sigma_2 f_{2l} - (\alpha_{1u1u2l}f^2_{1u} + \alpha_{1l1l2l}f^2_{1l} \\ & + 2\alpha_{1u1l2l}f_{1u}f_{1l})e^{+i\delta t}. \end{aligned} \tag{17}$$

Here the group velocity

$$v_{mg} = iv_{mlu} = -iv_{mul} \tag{18}$$

is defined to be real, as can be ascertained from the definition of v_{mlu} in Eq. (10); the frequency mismatch δ resulting from the material dispersion of the constituents of the structure is given by

$$\delta = \omega_{20} - 2\omega_{10}, \tag{19}$$

and the nonlinear overlap integrals α are defined through

$$\alpha_{1a1b2c} = \omega_{10}n_0^{1/2}\int_0^d \chi^{(2)}_{\text{eff}}(z)\phi_{1a}\phi_{1b}\phi^*_{2c}dz. \tag{20}$$

From this definition, $\alpha_{1u1l2u} = \alpha_{1l1u2u}$ and $\alpha_{1u1l2l} = \alpha_{1l1u2l}$. In the nonlinear terms in Eqs. (17) we have taken $\omega_{20} = 2\omega_{10}$ and $v_g = v_{1g} = v_{2g}$. Even though these are only approximate equalities because of dispersion, in our method these approximations are small corrections to the highest order terms included in the multiple scales calculation, and they thus lead to errors at orders which we have neglected in the first place.

Before discussing Eqs. (17) we note that since we take the FF and SHF to be tuned closely to the first and second grating-induced band gaps, from here on we use a field expansion about $k = \pi/d$ at the FF and $k = 0$ at the SHF respectively. At these positions in the BZ, the group velocity vanishes, leading to Bloch functions which are real and which have a definite parity. Thus we expect some of the α's in Eqs. (17) to vanish. A detailed discussion of these is given in Sec. V after casting Eqs. (17) into another form.

III. TRANSFORMATION TO COUPLED-MODE EQUATIONS

Equations (17) attain a more familiar form if we set

$$\begin{aligned} \mathcal{E}_{1\pm} &= \frac{1}{2}(f_{1l} \mp if_{1u}), \\ \mathcal{E}_{2\pm} &= \frac{1}{2}(f_{2l} \mp if_{2u})e^{i\delta t}. \end{aligned} \tag{21}$$

Applying this transformation to Eqs. (17), we find

$$\begin{aligned} & +i\frac{\partial \mathcal{E}_{1+}}{\partial z} + \frac{i}{v_{1g}}\frac{\partial \mathcal{E}_{1+}}{\partial t} + \kappa_1\mathcal{E}_{1-} + \Gamma_1\mathcal{E}^*_{1+}\mathcal{E}_{2+} + \Gamma_2\mathcal{E}^*_{1+}\mathcal{E}_{2-} \\ & \quad + \Gamma_3\mathcal{E}^*_{1-}\mathcal{E}_{2+} + \Gamma^*_3\mathcal{E}^*_{1-}\mathcal{E}_{2-} = 0, \\ & -i\frac{\partial \mathcal{E}_{1-}}{\partial z} + \frac{i}{v_{1g}}\frac{\partial \mathcal{E}_{1-}}{\partial t} + \kappa_1\mathcal{E}_{1+} + \Gamma_3\mathcal{E}^*_{1+}\mathcal{E}_{2+} + \Gamma^*_3\mathcal{E}^*_{1+}\mathcal{E}_{2-} \\ & \quad + \Gamma^*_2\mathcal{E}^*_{1-}\mathcal{E}_{2+} + \Gamma^*_1\mathcal{E}^*_{1-}\mathcal{E}_{2-} = 0, \\ & +i\frac{\partial \mathcal{E}_{2+}}{\partial z} + \frac{i}{v_{2g}}\frac{\partial \mathcal{E}_{2+}}{\partial t} + \delta k\mathcal{E}_{2+} + \kappa_2\mathcal{E}_{2-} + \Gamma^*_1\mathcal{E}^2_{1+} + \Gamma_2\mathcal{E}^2_{1-} \\ & \quad + 2\Gamma^*_3\mathcal{E}_{1+}\mathcal{E}_{1-} = 0, \\ & -i\frac{\partial \mathcal{E}_{2-}}{\partial z} + \frac{i}{v_{2g}}\frac{\partial \mathcal{E}_{2-}}{\partial t} + \delta k\mathcal{E}_{2-} + \kappa_2\mathcal{E}_{2+} + \Gamma^*_2\mathcal{E}^2_{1+} + \Gamma_1\mathcal{E}^2_{1-} \\ & \quad + 2\Gamma_3\mathcal{E}_{1+}\mathcal{E}_{1-} = 0, \end{aligned} \tag{22}$$

where $\mathcal{E}_{m\pm}$ refer to forward and backward propagating envelopes, $\delta k = \delta/v_{2g}$ is the wave number mismatch, and the linear coupling coefficient is given by

$$\kappa_m = \frac{\sigma_m}{v_{mg}}. \tag{23}$$

The nonlinear coefficients

$$\Gamma_j = \frac{1}{2v_g}(\beta_j + i\beta_{j+3}), \tag{24}$$

where β_j and β_{j+3}, for $j = 1-3$, are linear combinations of α_{1a1b2c}:

$$\begin{aligned}
\beta_1 &= \alpha_{1l1l2l} + 2\alpha_{1u1l2u} - \alpha_{1u1u2l}, \\
\beta_2 &= \alpha_{1l1l2l} - 2\alpha_{1u1l2u} - \alpha_{1u1u2l}, \\
\beta_3 &= \alpha_{1l1l2l} + \alpha_{1u1u2l}, \\
\beta_4 &= -\alpha_{1u1u2u} - 2\alpha_{1u1l2l} + \alpha_{1l1l2u}, \\
\beta_5 &= \alpha_{1u1u2u} - 2\alpha_{1u1l2l} - \alpha_{1l1l2u}, \\
\beta_6 &= \alpha_{1u1u2u} + \alpha_{1l1l2u}.
\end{aligned} \tag{25}$$

All β_j are real because all α's are real. We note that although Γ_{1-3} [Eqs. (24)] are complex, Eqs. (22) satisfy the condition

$$\begin{aligned}
&\frac{\partial}{\partial z}[(|\mathcal{E}_{1+}|^2 + |\mathcal{E}_{2+}|^2) - (|\mathcal{E}_{1-}|^2 + |\mathcal{E}_{2-}|^2)] \\
&\quad = \frac{\partial}{\partial t}\left[\frac{1}{v_{1g}}(|\mathcal{E}_{1+}|^2 + |\mathcal{E}_{1-}|^2) + \frac{1}{v_{2g}}(|\mathcal{E}_{2+}|^2 + |\mathcal{E}_{2-}|^2)\right].
\end{aligned} \tag{26}$$

This implies that

$$\frac{1}{v_{1g}}(|\mathcal{E}_{1+}|^2 + |\mathcal{E}_{1-}|^2) + \frac{1}{v_{2g}}(|\mathcal{E}_{2+}|^2 + |\mathcal{E}_{2-}|^2) \tag{27}$$

is conserved. Note that the quantity in Eq. (27) is also conserved in a lossless, uniform dispersive medium where neither a grating or a nonlinearity are present. To ensure that Eqs. (22) satisfy this condition, it was essential that we made the approximations discussed after Eq. (20).

IV. PROPERTIES OF THE BLOCH FUNCTIONS

In this section we discuss some of the important features of the parameters in Eqs. (22). We consider a periodic stack consisting of layers of GaAs and AlAs. The GaAs layers have a thickness d_{GaAs}, while the AlAs layers have a thickness d_{AlAs}. For this thin-film stack we choose to demonstrate our results at a wavelength $\lambda_{\mathrm{FF}} = 1.6\,\mu$m corresponding to a SH wavelength $\lambda_{\mathrm{SHF}} = 0.8\,\mu$m. At these wavelengths both GaAs and AlAs are known to be transparent at low temperatures. The refractive indices in each of the layers are $n_{1\mathrm{GaAs}} = 3.37$, $n_{1\mathrm{AlAs}} = 2.88$, $n_{2\mathrm{GaAs}} = 3.67$, and $n_{2\mathrm{AlAs}} = 3.04$ [26,27]. For this system, Fig. 3 shows the frequencies [in units of c/d] of the upper and lower band edges, for the first and second grating-induced band gaps, as a function of the GaAs filling fraction d_{GaAs}/d, where the period $d = d_{\mathrm{GaAs}} + d_{\mathrm{AlAs}}$.

In Fig. 3 the second grating-induced band gap vanishes at

$$\tilde{d} = \frac{n_{2\mathrm{AlAs}}}{n_{2\mathrm{AlAs}} + n_{2\mathrm{GaAs}}}\, d, \tag{28}$$

indicated by the dashed vertical line. For $\lambda_{FF} = 1.6\,\mu$m, Eq. (28) gives $\tilde{d}/d = 0.453$, consistent with Fig. 3. This effect of vanishing reflectivity is well known in the theory of thin-film stacks, and corresponds to the situation in which both the GaAs and AlAs layers have a wave thickness of $\lambda/2$ [20]. The disappearance of the band gap occurs because the contributions to the reflectivity from the even numbered interfaces exactly cancel those from the odd ones.

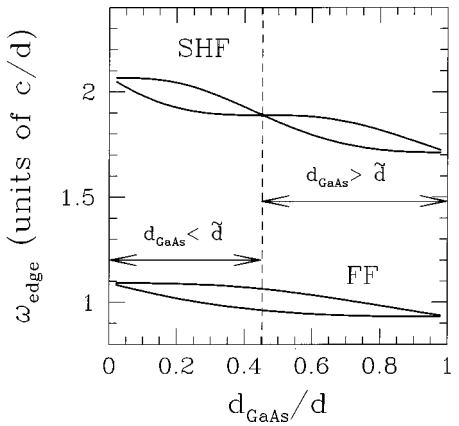

FIG. 3. The frequencies (in units of c/d) of the upper and lower band edges as a function of the GaAs filling fraction d_{GaAs}/d for the FF and SHF band gaps. The dashed vertical line at $d_{\mathrm{GaAs}} = \tilde{d}$ shows the period composition for which the band gap at the SHF vanishes.

Figures 4 and 5 show the Bloch functions for two GaAs-AlAs periodic structures at two different compositions. For Fig. 4, $d_{\mathrm{GaAs}} = 0.1$ and $d_{\mathrm{AlAs}} = 0.9$ (i.e., $d_{\mathrm{GaAs}} < \tilde{d}$), while for Fig. 5 $d_{\mathrm{GaAs}} = 0.9$ and $d_{\mathrm{AlAs}} = 0.1$ (i.e., $d_{\mathrm{GaAs}} > \tilde{d}$). As mentioned earlier, all Bloch functions are real, as required at the edge and the center of the BZ. The Bloch functions at the FF have a period twice that of the lattice period since $k = \pi/d$, while those at the SHF have the same periodicity as the lattice since $k = 0$. Note that in the center of the two layers the Bloch functions always have either a node or an antinode. At the first grating-induced band gap we find that ϕ_{1l} (ϕ_{1u}) always has a node (antinode) in the center of the low-index AlAs (high-index GaAs) layer. In contrast, at the second grating-induced band gap the position of the node of a particular Bloch function depends on whether $d_{\mathrm{GaAs}} < \tilde{d}$ or $d_{\mathrm{GaAs}} > \tilde{d}$. A summary of the nodes and antinodes of the relevant Bloch functions is given in Table I. The results in this table show that the Bloch functions at the second

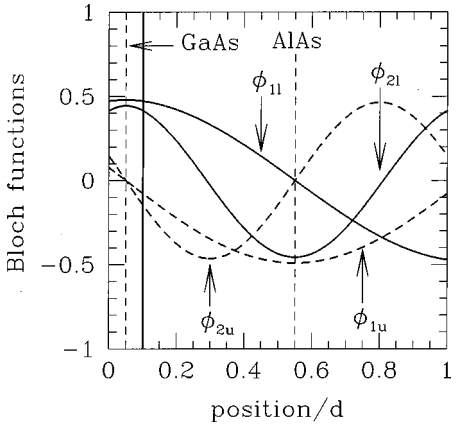

FIG. 4. Bloch functions (as labeled) for a GaAs-AlAs periodic structure with $d_{\mathrm{GaAs}} = 0.1$ and $d_{\mathrm{AlAs}} = 0.9$. Note that in the center of d_{GaAs}, ϕ_{mu} have nodes, while ϕ_{ml} have antinodes, for $m = 1$ and 2.

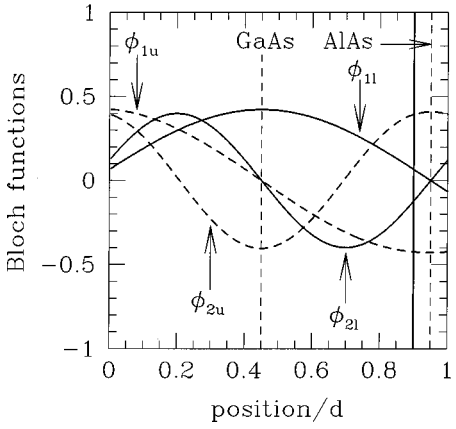

FIG. 5. The Bloch functions (as labeled) for a GaAs-AlAs periodic structure with $d_{\mathrm{GaAs}}=0.9$ and $d_{\mathrm{AlAs}}=0.1$. Here $\phi_{1l,u}$ have nodes and antinodes as in Fig. 4, while $\phi_{2l,u}$ now have a node and an antinode in the center of d_{GaAs}.

grating-induced band gap reverse roles on adjacent sides of $\tilde{d}$.

V. STANDARD COUPLED-MODE EQUATIONS: SHALLOW GRATING LIMIT

We now turn to consider the shallow grating limit of our results when $d_{\mathrm{GaAs}}/d\rightarrow 0,1$. The two compositions in Figs. 4 and 5 were chosen to show the features of this case. In this limit the Bloch functions can be written as simple trigonometric functions. Choosing the origin to be in the center of the high-index GaAs layer, the Bloch functions are given by

$$\phi_{1l}=+a_{1l}\cos\left(\frac{\pi z}{d}\right),\quad \phi_{1u}=-a_{1u}\sin\left(\frac{\pi z}{d}\right),$$

$$d_{\mathrm{GaAs}}<\tilde{d}:\phi_{2l}=+a_{2l}\cos\left(\frac{2\pi z}{d}\right),\quad \phi_{2u}=-a_{2u}\sin\left(\frac{2\pi z}{d}\right), \tag{29}$$

$$d_{\mathrm{GaAs}}>\tilde{d}:\phi_{2l}=-a_{2l}\sin\left(\frac{2\pi z}{d}\right),\quad \phi_{2u}=-a_{2u}\cos\left(\frac{2\pi z}{d}\right),$$

where $a_{ml,u}$ are the Bloch function amplitudes which follow from normalization [21], and where the signs of the Bloch functions are chosen such that $v_{mg}>0$. Using Eqs. (29) in Eqs. (25), (20), and (24), we find

TABLE I. Comparison of the nodes and antinodes of the Bloch functions in the centers of the high-index d_{GaAs} and low-index d_{AlAs} layers for $d_{\mathrm{GaAs,AlAs}}<\tilde{d}$ and $d_{\mathrm{GaAs,AlAs}}>\tilde{d}$.

	$d_{\mathrm{GaAs}}<\tilde{d}$		$d_{\mathrm{GaAs}}>\tilde{d}$	
Bloch function	high n	low n	high n	low n
ϕ_{1l}	antinode	node	antinode	node
ϕ_{1u}	node	antinode	node	antinode
ϕ_{2l}	antinode	antinode	node	node
ϕ_{2u}	node	node	antinode	antinode

$$d_{\mathrm{GaAs}}<\tilde{d}:$$

$$\alpha_{1l1l2l}=\alpha_{1l1u2u}=-\alpha_{1u1u2l},$$

$$\beta_1=4\alpha_{1l1l2l},$$

$$\Gamma_1=\beta_1/(2v_g)=\sqrt{2n_0}\,c\pi\overline{\chi^{(2)}_{\mathrm{eff}}}/\left(\overline{n_1^3}\overline{n_2}v_g d^{3/2}\right); \tag{30}$$

$$d_{\mathrm{GaAs}}>\tilde{d}:$$

$$\alpha_{1u1u2u}=\alpha_{1u1l2l}=-\alpha_{1l1l2u},$$

$$\beta_4=-4\alpha_{1u1u2u},$$

$$\Gamma_1=i\beta_4/(2v_g)=-i\sqrt{2n_0}\,c\pi\overline{\chi^{(2)}_{\mathrm{eff}}}/\left(\overline{n_1^3}\overline{n_2}v_g d^{3/2}\right);$$

and all others vanish. Here, $\overline{n_{1,2}}$ are the average refractive indices at the FF and SHF, and $\overline{\chi^{(2)}_{\mathrm{eff}}}$ is the period average of the effective quadratic nonlinearity [23–25]. Clearly, the only nonlinear coefficient which survives in this limit is Γ_1. Note that $|\Gamma_1|$ is a continuous function of composition, but with a phase jump of $-\pi/2$ at $d_{\mathrm{GaAs}}=\tilde{d}$. Substituting Eqs. (30) into Eqs. (22), we find

$$\begin{aligned}
&+i\frac{\partial\mathcal{E}_{1+}}{\partial z}+\frac{i}{v_{1g}}\frac{\partial\mathcal{E}_{1+}}{\partial t}+\kappa_1\mathcal{E}_{1-}+(i)\Gamma_1\mathcal{E}^*_{1+}\mathcal{E}_{2+}=0,\\
&-i\frac{\partial\mathcal{E}_{1-}}{\partial z}+\frac{i}{v_{1g}}\frac{\partial\mathcal{E}_{1-}}{\partial t}+\kappa_1\mathcal{E}_{1+}+(-i)\Gamma_1\mathcal{E}^*_{1-}\mathcal{E}_{2-}=0,\\
&+i\frac{\partial\mathcal{E}_{2+}}{\partial z}+\frac{i}{v_{2g}}\frac{\partial\mathcal{E}_{2+}}{\partial t}+\delta k\mathcal{E}_{2+}+\kappa_2\mathcal{E}_{2-}+(-i)\Gamma_1\mathcal{E}^2_{1+}=0,\\
&-i\frac{\partial\mathcal{E}_{2-}}{\partial z}+\frac{i}{v_{2g}}\frac{\partial\mathcal{E}_{2-}}{\partial t}+\delta k\mathcal{E}_{2-}+\kappa_2\mathcal{E}_{2+}+(i)\Gamma_1\mathcal{E}^2_{1-}=0,
\end{aligned} \tag{31}$$

where the factors in brackets should be ignored for $d_{\mathrm{GaAs}}<\tilde{d}$. For $d_{\mathrm{GaAs}}>\tilde{d}$ the bracketed terms should be included; otherwise all parameters have the same values. Alternatively, applying transformation $\mathcal{A}_{2\pm}=\pm i\mathcal{E}_{2\pm}$ to Eqs. (31) for $d_{\mathrm{GaAs}}>\tilde{d}$ shows that the parameters for $d_{\mathrm{GaAs}}<\tilde{d}$ and $d_{\mathrm{GaAs}}>\tilde{d}$ can be made to be identical, except for the sign of κ_2. Therefore, the solutions on adjacent sides of $\tilde{d}$ are not necessarily straightforwardly related to each other.

Equations (31) are identical to the coupled-mode equations obtained by He and Drummond [9]. Also, by using a transformation slightly different from that used in Eqs. (21), it can be shown that Eqs. (31) have a form identical to that used recently in Ref. [10]. In Refs. [9–11] solutions to Eqs. (31) are also given.

VI. COUPLED-MODE COEFFICIENTS FOR DEEP GRATINGS

We now consider the full Eqs. (22). The most obvious difference between Eqs. (22) and those obtained in Refs.

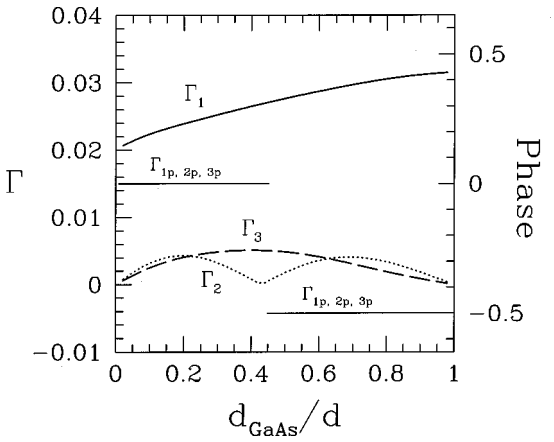

FIG. 6. Amplitude Γ_s [in units of $c\chi^{(2)}_{\rm eff}/(v_g d^{3/2})$ where $\chi^{(2)}_{\rm eff}$ is that of GaAs] and phase Γ_{jp} (in units of π) of the nonlinear coefficients, for $j=1-3$, as a function of the filling fraction of GaAs for a GaAs-AlAs periodic stack. Here $n_{1\rm GaAs}=3.37$, $n_{1\rm AlAs}=2.88$, $n_{2\rm GaAs}=3.67$, $n_{2\rm AlAs}=3.04$, and $n_0=1$ and $\chi^{(2)}_{\rm AlAs}/\chi^{(2)}_{\rm GaAs}=0.33$.

[9,10] is the two additional nonlinear coefficients Γ_2 and Γ_3. These coefficients introduce the nonlinear coupling between the forward and backward propagating other modes at the FF and SHF. Another point to note is that the coefficients here have different values compared to the equivalent terms in Refs. [9]. For example, in Eqs. (22), the linear coupling coefficient κ_m is given in terms of the exact eigenvalues and eigenfunctions of the linear system [Eq. (23)]. In contrast, the coupling coefficient for Nth order Bragg reflection for shallow gratings is $\kappa=\pi\Delta n/\lambda$, where Δn is the Nth order Fourier amplitude of the refractive index [9]. Note that, as was the case in the shallow limit, $|\Gamma_{1-3}|$ are continuous functions of $d_{\rm GaAs}$, but that the phases of Γ_{1-3} exhibit jumps at $\tilde{d}$; we discuss these in more detail in the example below.

Though the results derived are perfectly general, we now continue our example of a GaAs-AlAs stack at $\lambda_{\rm FF}=1.6$ μm. The linear properties were already discussed in Sec. IV. Further, from symmetry considerations it is well known that for GaAs and AlAs, the nonlinear $\chi^{(2)}$ tensor has six nonzero elements, all of which have the same value [23,24]. In the commonly used contracted d_{il} notation these elements are $d_{14}=d_{25}=d_{36}$ [23,24]. Our example applies to the geometry of van der Ziel and Illegems [28]. With a GaAs-$Al_{0.3}Ga_{0.7}As$ multilayer, cut in the [110] direction, and an incident FF beam with polarization parallel to the [110] axis, a colinear SHF field is generated, polarized in the [001] plane [28]. For this geometry and field polarization only the d_{36} elements of GaAs and AlAs are relevant. Using Miller's rule, we take the d_{36} ratio between AlAs and GaAs to be 0.33 [23]. For consistency with current literature [9–11], below we use a $\chi^{(2)}$ notation; the relation to the d_{il} tensor is straightforward [23].

Figure 6 shows the magnitudes of Γ_{1-3} [in units of $c\chi^{(2)}_{\rm GaAs}/(v_g d^{3/2})$], using the left-hand vertical scale, and their phases [in units of π], using the right-hand scale, versus $d_{\rm GaAs}/d$. The magnitude of the Γ's are labeled as Γ_{1-3}, the phases are labeled as Γ_{1p-3p}. As in the shallow grating case, the phases of Γ_{1-3} change by $-\pi/2$ at $d_{\rm GaAs}=\tilde{d}$, since ϕ_{2l} and ϕ_{2u} reverse roles here. The coefficient Γ_1 remains the dominant coefficient. Although Γ_2 and Γ_3 are certainly smaller we find that $\Gamma_2=0.18\Gamma_1$ and $\Gamma_3=0.20\Gamma_1$ at $d_{\rm GaAs}/d=0.18$ and $d_{\rm GaAs}/d=0.34$, respectively. Note that in the shallow grating limit, when $d_{\rm GaAs}/d\to 0$ (1), Fig. 6 shows that, in the units used, $\Gamma_1=0.021$ ($\Gamma_1=0.031$) and $\Gamma_{2,3}\to 0$. These values are consistent with Eqs. (30). As a final comment, we note that in many experiments, the fields are not polarized along crystal axes; in such cases one should use $\chi^{(2)}_{\rm eff}$, corresponding to a suitably weighted average over the nonzero tensor elements [23,24]. Kobyakov, Peschel, and Lederer gave a detailed discussion of, and expressions for, $\chi^{(2)}_{\rm eff}$ for both type I and type II SHG [25].

VII. DISCUSSION AND CONCLUSIONS

We have considered periodic media with a second-order nonlinearity, where the FF and SHF fields are close to the first and second Bragg resonances of the structure. However, in addition to this, in many geometries the SHF may be scattered out of the plane by the first-order resonance as well. Though this is completely avoided in thin-film geometries [29–31], it needs to be considered in guided-wave geometries, where it effectively leads to a loss at the SHF. However, in waveguide geometries this loss can be minimized by designing the cover and the cladding regions as a multilayer which reflects the scattered out of plane SH back toward the waveguide in phase with the original SHF guided mode [31].

In our derivation we have taken the fields to be concentrated around the lowest band gaps of a deep grating. One could, for example, also consider a situation with two gratings 1 and 2 with periods $d_1\approx 2d_2$ and for grating 1, $d_{\rm GaAs}=\tilde{d}$. In this case the FF would see grating 1 and the SHF would see only grating 2. The photonic band structures for the FF and SHF would then have no necessary relations, thus greatly enhancing the design flexibility.

The main results of our derivation were demonstrated for a stack consisting of layers of GaAs and AlAs. In applying our results to such structures, we note that in practice these gratings are only of the order of 50 periods. Although such structures may seem short, these lengths are sufficient to demonstrate the basic effects of nonlinear pulse propagation using femtosecond pulses because of the depth of the grating.

In conclusion, we have presented a systematic approach based on a Bloch function expansion and the method of multiple scales [21], to analyze light propagation for type I interaction in quadratically nonlinear periodic media. In our derivation we arrive at a set four coupled-mode equations which look similar to the standard coupled-mode equations [9–11], except that the values of some of the coefficients are different and that some additional nonlinear terms arise. These equations meet the conservation of energy condition required for a lossless medium under two approximations which are well justified within our formalism. Our results show that for the composition $d_{\rm GaAs}=\tilde{d}$ [see Eq. (28)] of the periodic structure, the second grating-induced band gap vanishes, in agreement with well known results in the theory of thin-film stacks [20]. As a consequence, even though the magnitudes of the nonlinear coefficients Γ_{1-3} are continuous, their phases jump by $-\pi/2$ at $d_{\rm GaAs}=\tilde{d}$. Thus, we

would expect that the solutions to Eqs. (22), for $d_{\mathrm{GaAs}}<\tilde{d}$ and $d_{\mathrm{GaAs}}>\tilde{d}$, not to be straightforwardly related. Finally, soliton solutions to Eqs. (31) have been found by many authors [9–11]; however, these are unlikely to be solutions to Eqs. (22). We will address solutions to these equations in future publications.

ACKNOWLEDGMENTS

We thank Dr. H. He and Professor T. G. Brown for discussions about this work. This work was supported by the Australian Research Council. A.A. was supported by the Australian Postgraduate Award Scheme and by the Australian Photonics Cooperative Research Centre.

[1] C. M. de Sterke and J. E. Sipe, in *Progress in Optics*, edited by E. Wolf (North-Holland, Amsterdam, 1994), Vol. XXXIII, pp. 203–260 (1994).
[2] B. J. Eggleton, R. E. Slusher, C. M. de Sterke, P. A. Krug, and J. E. Sipe, Phys. Rev. Lett. **76**, 1627 (1996).
[3] L. F. Mollenauer, R. H. Stolen, and J. P. Gordon, Phys. Rev. Lett. **45**, 1095 (1980).
[4] G. P. Agrawal, *Nonlinear Fiber Optics* (Academic, San Diego, 1989).
[5] Y. N. Karamzin and A. P. Sukhorukov, Zh. Éksp. Teor. Fiz. **68**, 834 (1975) [Sov. Phys. JETP **41**, 414 (1976)].
[6] A. V. Buryak and Y. S. Kivshar, Opt. Lett. **19**, 1612 (1994).
[7] P. Agin and G. I. Stegeman, J. Opt. Soc. Am. B **14**, 3162 (1997).
[8] A. V. Buryak, Y. S. Kivshar, and S. Trillo, J. Opt. Soc. Am. B **14**, 3110 (1997).
[9] H. He and P. D. Drummond, Phys. Rev. Lett. **78**, 4311 (1997).
[10] C. Conti, S. Trillo, and G. Assanto, Phys. Rev. E **57**, 1251R (1998); Opt. Lett. **23**, 334 (1998).
[11] T. Peschel, U. Peschel, F. Lederer, and B. A. Malomed, Phys. Rev. E **55**, 4730 (1997).
[12] W. E. Torruellas, Z. Wang, D. J. Hagan, E. W. VanStryland, G. I. Stegeman, L. Torner, and C. R. Menyuk, Phys. Rev. Lett. **74**, 5036 (1995).
[13] R. Schiek, Y. Baek, and G. Stegeman, Phys. Rev. E **53**, 1138 (1996).
[14] R. A. Fuerst, M. T. G. Canva, and G. I. Stegeman, Opt. Lett. **22**, 1748 (1997).
[15] M. T. G. Canva, R. A. Fuerst, S. Baboiu, and G. I. Stegeman, Opt. Lett. **55**, 1683 (1997).
[16] P. Di Trapani, D. Caironi, G. Vaiulis, A. Dubietis, R. Danielius, and A. Piskaskas, Phys. Rev. Lett. **81**, 570 (1998).
[17] C. Conti, S. Trillo, and G. Assanto, Opt. Lett. **22**, 445 (1997).
[18] M. Scalora, M. J. Bloemer, A. S. Manka, J. P. Dowling, C. M. Bowden, R. Viswanthan, and J. W. Haus, Phys. Rev. A **56**, 3166 (1997).
[19] D. Marcuse, *Theory of Dielectric Optical Waveguides*, 2nd ed. (Academic, Boston, 1991).
[20] H. A. Macleod, *Thin-Film Optical Filters*,, 2nd ed. (Hilger, Birmingham, 1984).
[21] C. M. de Sterke, D. G. Salinas, and J. E. Sipe, Phys. Rev. E **54**, 1969 (1996).
[22] J. E. Sipe, L. Poladian, and C. M. de Sterke, J. Opt. Soc. Am. A **11**, 1307 (1994).
[23] R. W. Boyd, *Nonlinear Optics* (Academic, San Diego, 1992).
[24] R. L. Sutherland, *Handbook of Nonlinear Optics* (Dekker, New York, 1996).
[25] A. Kobyakov, U. Peschel, and F. Lederer, Opt. Commun. **124**, 184 (1996).
[26] H. C. Casey, J. R. Panish, and M. B. Panish, *Heterostructure Laser* (Academic, New York, 1978).
[27] *Optical Properties of III-V Compounds*, edited by R. K. Willardson and A. C Beer, Semiconductors and Semimetals Vol. 3 (Academic, New York, 1967).
[28] J. P. van der Ziel and M. Illegems, Appl. Phys. Lett. **28**, 437 (1976).
[29] W. Streifer, D. R. Scifres, and R. D. Burnham, IEEE J. Quantum Electron. **12**, 422 (1976).
[30] W. Streifer, D. R. Scifres, and R. D. Burnham, IEEE J. Quantum Electron. **12**, 494 (1976).
[31] A. Hardy, D. F. Welch, and W. Streifer, IEEE J. Quantum Electron. **25**, 2096 (1989).